Proceedings of the 18th International Conference on Soil Mechanics and Geotechnical Engineering, Paris 2013

Parallel session ISP 6

Analysis of Self-boring Pressuremeter Tests in a Sensitive Clay of Quebec

Analyse d'essais au pressiométre auto-foreur dans une argile sensible au Québec

V. Silvestri
Department of civil engineering, Ecole Polytechnique, Montreal, Quebec, Canada
C. Tabib
Consultant, Montreal, Quebec, Canada

ABSTRACT : The present paper analyzes self-boring pressuremeter test results obtained in a clay deposit of Quebec. The clay is lightly overconsolidated and sensitive. Stress-strain curves were first determined using both a linearly elastic perfectly plastic model and a nonlinear plastic model based on total stress analysis. Additional stress-strain curves were then obtained using relationships based on the application of modified Cam clay. This approach allowed the determination of effective radial, axial, and tangential stresses as well as effective stress paths and distributions in the soil surrounding the expanding cylindrical cavity.

RÉSUMÉ : Cet article présente les résultats d'essais au pressiomètre autoforeur obtenus dans un dépôt d'argile du Québec. L'argile est surconsolidée et sensible. Des relations contraintes-déformations ont été d'abord obtenues à l'aide d'analyses en contraintes totales en utilisant soit un modèle linéaire élastique parfaitement plastique soit un modèle non-linéaire plastique. Des relations additionnelles ont été par la suite obtenues en utilisant le modèle Cam clay modifié. Cette dernière approche a permis de déterminer les contraintes effectives radiale, axiale, et tangentielle, ainsi que les cheminements des contraintes et leurs distributions dans le sol pendant l'expansion de la cavité cylindrique.

KEYWORDS : Self-boring pressuremeter tests, sensitive clay, modified Cam clay, stress-strain curves, stress distributions and paths.
MOTS-CLÉS : essais au pressiomètre auto-foreur, argile sensible, modèle Cam-clay modifié, courbes effors-déformation, répartition des contraintes, chemin de contraintes.

1 INTRODUCTION

The interpretation of pressuremeter tests in clay is generally carried out using a total stress approach by means of either a classical elastic-plastic or a non-linear plastic analysis (Cassan 1960; Gibson and Anderson 1961; Baguelin et al. 1972; Ladanyi 1972; Palmer 1972). However, Randolph et al. (1979) showed by employing a finite element analysis that the modified Cam clay model could be used to determine effective stresses and pore pressures generated in the soil surrounding the cylindrical cavity.

Up to quite recently, geotechnical investigators were under the impression that an exact solution could not be obtained for the effective stresses and strains generated arround a pressuremeter probe expanded in modified Cam clay. However, Chen and Abousleiman (2012) and Silvestri and Abou-Samra (2012) independently derived such a solution, thereby rendering unnecessary the use of a finite element analysis.

This paper presents the results of a series of self-boring pressuremeter tests carried out in an overconsolidated sensitive clay deposit of Quebec. Constitutive relationships determined by the total stress approach are compared with those derived from a modified version of the effective stress solution obtained by Silvestri and Abou-Samra (2012). It is shown that the effective stress approach allows obtaining the complete description of the soil response. The derived stress-strain relationships are different from those found from application of a total stress analysis.

2 FIELD TEST RESULTS

Several self-boring pressuremeter (SBPM) tests were carried out in an overconsolidated sensitive clay deposit of Quebec. The pressuremeter probe used was a Cambridge, Mark VIII model, equipped with pore pressure gauges. Tests were performed below the oxidized crust to a maximum depth of 15 m. The overconsolidation ratio of the clay deposit decreases with depth, varying from about 5.5 below the crust to 2.4 in the deeper soil layers. While the natural moisture content ranges from 65 to 80%, the plastic and liquid limits average 25 and 68%, respectively. The in-situ undrained shear strength was determined by means of vane tests and was found to vary linearly with depth, from 30 kPa at 3 m to 50 kPa at 15 m. The water table is close to the ground surface.

The in-situ geostatic stress, σ_{ho},was deduced from SBPM tests, Marchetti dilatometer (MD) tests, and hydraulic fracturing (HF) tests. The computed in-situ coefficient of lateral earth pressure at rest, K_o, was found to be extremely high, with SBPM-derived values ranging between 2.1 below the crust and 1.3 in the deeper layers, compared to MD-derived values of 1.5-0.9, and HF-derived values of 1.8-1.2. The SBPM-based lift-off pressures were computed from the average of the responses of the three feeler arms. However, as the feeler arms showed large differences in strains and in apparent lift-off pressures, large uncertainties resulted in the estimation of K_o. Because one of the feeler arms consistently led to an apparent lift-off pressure of more than 45% of the average value deduced from the remaining arms, the test measurements were re-considered and resulted in better estimates of K_o, For instance, a value of $K_o \simeq 1$ was computed from the SBPM tests carried out at 6 m, instead of the originally determined value of 1.6.

Typical SBPT tests results obtained at 6 m are presented in Figure 1. The slope of the linear portion of the expansion curves versus the logarithm of the shear strain γ allows the determination of the undrained shear strength S_u. An average value of 50 kPa is obtained for S_u at 6 m, as compared to 35 kPa found from the in-situ vane tests. The value of the shear modulus G' can also be derived from the expansion curves shown in Figure 1, if a linearly elastic perfectly plastic (Tresca) model is assumed for the soil response. This leads to an average value of G' of 5720 kPa. Expansion curves based on the Tresca model are compared in Fig.2 with the experimental curves. Examination of the reported relationships shows that the Tresca model gives a satisfactory fit to the data.

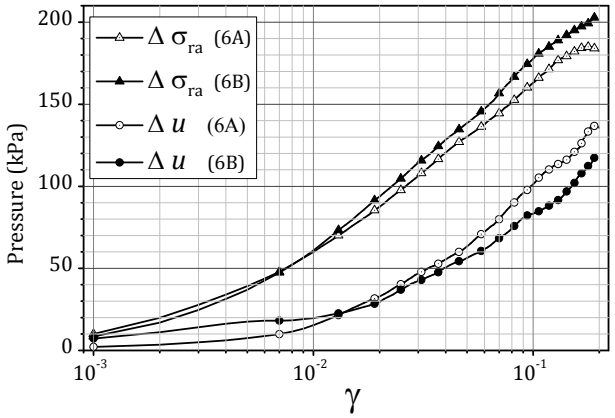

Figure 1. Typical expansion and excess pore pressure curves.

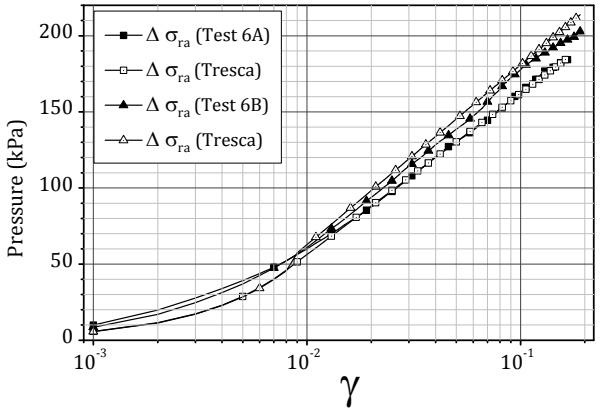

Figure 2. Comparison between experimental and Tresca-based expansion curves.

3 CAM CLAY PARAMETERS AND MODELLING

Triaxial tests were carried out on undisturbed specimens recovered at a depth of 6 m. The Cam clay parameters that were computed from the test results are the following: $v = 3.07$, $M = 1.2$, $\lambda = 0.65$, $\kappa = 0.03$, and $\Lambda = (\lambda - \kappa)/\lambda = 0.954$. The specific volume v equals $1 + e$, with $e =$ voids ratio; $M = 6sin\phi'/(3 - sin\phi')$ is the critical state parameter, with $\phi' = 30^{\circ}$; λ is the slope of the $v - lnp'$ relationship in loading, with $p' =$ mean effective stress; and κ is the slope of the $v - lnp'$ relationship in swelling.

The initial yield curve of the clay is described by the following equation

$$q = p'M\left(\frac{p'_c}{p'} - 1\right) \tag{1}$$

where $q =$ deviator stress, and p'_c is a hardening parameter which controls the size of the yield curve. For the clay recovered at 6 m, the initial value of p'_c equals 160 kPa. The effective stress path (ESP) followed by the clay when both elastic and plastic strains are occurring is given by (See Figure 3):

$$q = p'M\left[\left(\frac{p'_o}{p'}\right)^{\frac{1}{\Lambda}} - 1\right]^{\frac{1}{2}} \tag{2}$$

where p'_o, which equals 150.1 kPa in the present case, represents the value of p' for $q = 0$.

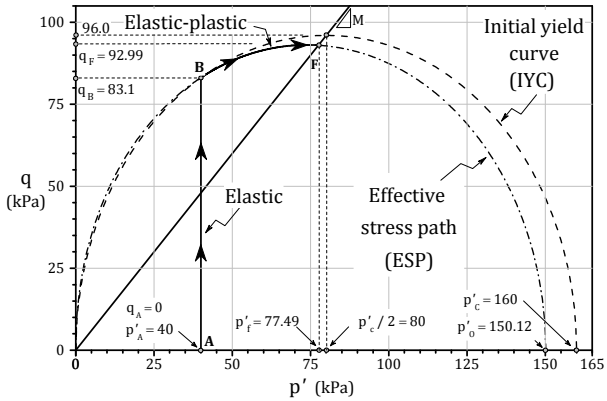

Figure 3. Effective stress path and initial yield curve of clay.

Because the clay is overconsolidated, the starting point of the ESP is represented by point A (*i.e.*, $p'_A = p'_i = \sigma'_{zi} = \sigma'_{ri} = \sigma'_{\theta i} = 40$ kPa, $q_A = q_i = \sigma'_{zi} - \sigma'_{ri} = 0$) which is located inside the initial yield locus, as shown in Figure 3. Note that the initial stress parameters are: $\sigma'_{ri} = \sigma'_{\theta i} = K_o\sigma'_{zi}$,$p'_i = (\sigma'_{zi} + \sigma'_{\theta i} + \sigma'_{ri})/3 = (1 + 2K_o)\sigma'_{zi}/3$, and $q = [(\sigma'_{ri} - \sigma'_{\theta i})^2 + (\sigma'_{\theta i} - \sigma'_{zi})^2 + (\sigma'_{zi} - \sigma'_{ri})^2]^{\frac{1}{2}}/\sqrt{2} = (1 - K_o)\sigma'_{zi}$. During the first phase of expansion, the ESP rises vertically until the clay yields at point B ($p'_B = p'_i = 40$ kPa, $q_B = 83.1$ kPa from Eq. 1). The segment AB represents the elastic response of the soil. The ESP then follows Eq. 2 for $p'_o = 150.1$ kPa from point B to point F at critical state. The coordinates of point F are $p'_F = 2^{-\Lambda}p'_o = 77.5$ kPa, $q_f = Mp'_f = 93.0$ kPa. The theoretical value of the undrained shear strength S_u at point F equals $q_f/\sqrt{3}$ (Randolph et al. 1979) or 53.7 kPa. In addition, the effective radial, vertical, and tangential stresses at critical state are given by: $\sigma'_{rf} = p'_f + q_f/\sqrt{3} = 131.2$ kPa, $\sigma'_{zf} = p'_f = 77.5$ kPa, $\sigma'_{\theta f} = p'_f + q_f/\sqrt{3} = 23.8$ kPa.

The principal effective stresses generated in the course of the expansion were computed using a modified form of the solution obtained by Silvestri and Abou-Samra (2012). The stresses are:

$$\sigma'_r = p' - \left(\frac{\sigma'_{zi} - p'_i}{2}\right)e^{\frac{6G'\kappa}{vM^2}F(p',p'_c)} + \tau \tag{3a}$$

$$\sigma'_z = p' + (\sigma'_{zi} - p'_i)e^{\frac{6G'\kappa}{vM^2}F(p',p'_c)} \tag{3b}$$

$$\sigma'_\theta = p' - \left(\frac{\sigma'_{zi} - p'_i}{2}\right)e^{\frac{6G'\kappa}{vM^2}F(p',p'_c)} - \tau \tag{3c}$$

where

$$\tau = \frac{1}{3}\left[\frac{4}{3}q^2 - 3(\sigma'_{zi} - p'_i)^2 e^{\frac{12G'}{vM^2}F(p',p'_c)}\right]^2 \tag{4a}$$

and

$$F(p', p_c') = \int_{p_i'}^{p'} \frac{dp'}{p'(2p'-p_c')} \quad (4b)$$

In addition, the shear strain γ is given by

$$\gamma = \frac{\tau}{G} - \frac{6\kappa}{vM^2} F(p', p_c') \quad (5)$$

The hardening parameter p_c' in the preceding equations decreases during shearing. It varies from an initial value of 160.0 kPa to a final value of 155.0 kPa or $2p_f'$ at critical state.

The theoretical stress-strain curve obtained from application of Eqs. 4 is reported in Figure 4. Examination of the curve shows that it is linear up to $\tau = 48$ kPa which coresponds to point B in Figure 3. The maximum value of the shear stress τ equals S_u or 53.7 kPa. Equations 4 allow the determination of the effective stresses and the pore pressure in the soil surrounding the cylindrical cavity. Figure 5 presents the distribution of stresses as function of the radial distance from the cavity. The ratio r'/a represents a relative radial distance, where r' is the radial distance after distortion and a is the unstrained radius of the cavity. The distributions presented in Figure 5 correspond to the instance when the strained radius of the cavity a' is equal to $2a$. According to Randolph *et al.* (1979), the effective stresses generated at the wall of the cavity would have practically reached their limiting values when $a' = 2a$. Examination of the curves in Figure 4 shows the following: a) the stresses in the clay surrounding the cavity remain elastic for radial distances r'/a in excess of 21, and b) there exists a region of tensile tangential stress comprised approximately between $r'/a = 12$ and $r'/a = 21$.

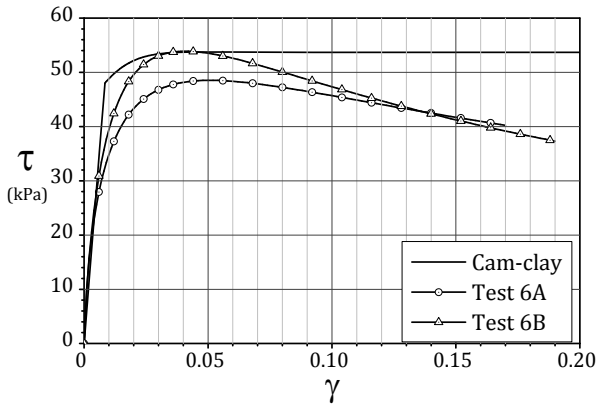

Figure 4. Stress-strain curves

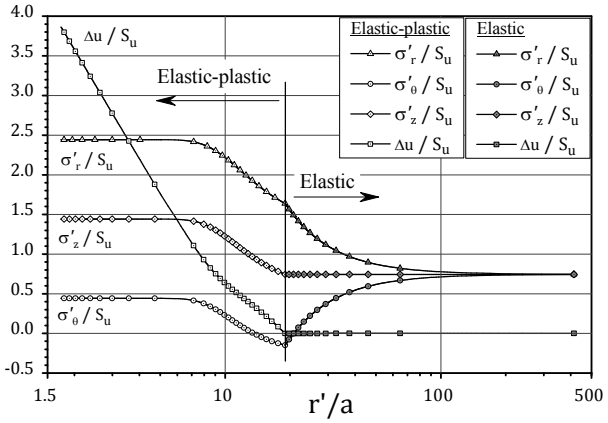

Figure 5. Stress distributions around cylindrical cavity.

4 ANALYSIS OF PRESSUREMETER TESTS

Shear stress-shear strain relationships were also derived from the expansion curves by means of Palmer's total stress approach (Palmer 1972):

$$\tau = \frac{d\sigma_{ra}}{dln\gamma} \quad (6)$$

where σ_{ra} is the applied expansion pressure. The curves are also reported in Figure 4. Comparison with the theoretical relationship derived using the effective stress approach indicates that the curve based on the experimental data fail to show the initial elastic response of the clay. It is evident that the shear modulus G' varies during the elastic phase of the expansion.

Once the shear stress τ is obtained as a function of the cavity shear strain γ, the tangential stress $\sigma_{\theta a}$ is found by noting that $\sigma_{\theta a} = \sigma_{ra} - 2\tau$. Corresponding effective stresses, σ'_{ra} and $\sigma'_{\theta a}$, are determined by substracting the observed pore pressures from the total stresses. Consequently, effective stress paths (ESPs) may be computed by using the parameters $s' = (\sigma'_{ra} + \sigma'_{\theta a})/2$ and $t' = (\sigma'_{ra} - \sigma'_{\theta a})/2$. ESPs can then be compared with that determined from application of Eqs. 4, as shown in Figure 6. Examination of the curves reported in this figure shows once again that the experimental-derived curves do not show the straight-line segments in the elastic phase of the expansion. Such response is caused by the variation of the shear modulus during shearing.

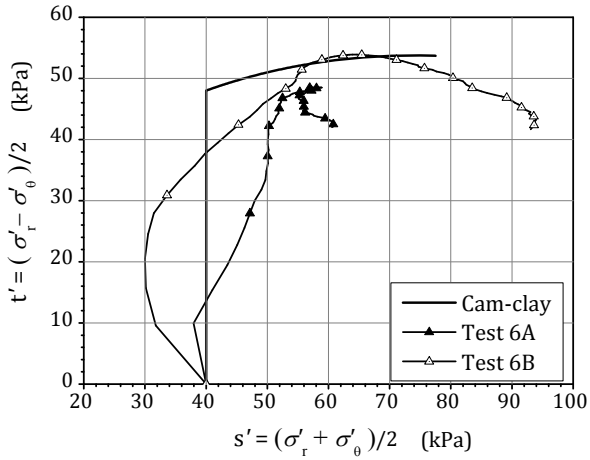

Figure 6. Comparison of effective stress paths

5 CONCLUSIONS

The following main conclusions are drawn on the basis of the findings in the present paper:

a) SBPM-deduced effective stress paths do not compare well with modified Cam clay-derived effective stress paths. The latter were computed by letting the hardening parameter p_c' vary during the expansion process, but by keeping constant the initial shear modulus.

b) Shear stress-shear strain relationships derived from Palmer's total stress approach are different from those determined using modified Cam clay.

c) The modified Cam clay model coupled with the effective stress analysis allows to determine the distribution of effective stresses and excess pore pressures generated in the soil surrounding the cavity.

d) For the particular case of $K_o = 1$, it is found that a zone of tensile effective tangential stress exists at some distance from the cavity.

6 ACKNOWLEDGEMENTS

The authors express their gratitude to the Natural Sciences and Engineering Research Council of Canada for the financial support received in the course of the present study.

7 REFERENCES

Baguelin, F., Jézéquel, J.F., Lemée, E., and Le Méhauté, A. 1972. Expansion of cylindrical probes in cohesive soils. Journal of the Soil Mechanics and Foundations Division, ASCE, 98(11): 1129-1142.

Cassan, M. 1960. Pressuremeter methods for the study of soils (In French). L'ingénieur-constructeur, May, pp. 3-16.

Chen, S.L., and Abousleiman, Y.N. 2012. Exact undrained elasto-plastic solution for cylindrical cavity expansion in modified Cam clay. Géotechnique, 62(5):447-456.

Gibson, R.E., and Anderson, W.F. 1961. In situ measurement of soil properties with the pressuremeter. Civil Engineering & Public Works Riview, 56(658):615-618.

Ladanyi, B. 1972. In-situ determination of undrained stress-strain behavior of sensitive clays with the pressuremeter. Canadian Geotechnical Journal, 9(3):313-319.

Palmer, A.C. 1972. Undrained plane strain expansion of a cylindrical cavity in clay: a simple interpretation of the pressuremeter test. Géotechnique, 22(3):451-457.

Silvestri, V., and Abou-Samra, G. 2012. Analytical solution for undrained plane strain expansion of a cylindrical cavity in modified Cam clay. Geomechanics and Engineering, 4(1): 19-37.

Randolph, M.F., Carter, J.P., and Wroth, C.P. 1979. Driven piles in clay-the effect of installation and subsequent consolidation. Géotechnique, 29(4):361-393.